

RESEARCH

Open Access



Nonlinear Frame Element with Shear–Flexure Interaction for Seismic Analysis of Non-Ductile Reinforced Concrete Columns

Worathep Sae-Long¹, Suchart Limkatanyu^{1*} , Woraphot Prachasaree¹, Suksun Horpibulsuk² and Pattamad Panedpojaman¹

Abstract

This paper presents and emphasizes the essence of inclusion of shear response and shear–flexure interaction in the investigation of reinforced concrete (RC) columns characterized by light and inadequately (substandard) detailed transverse reinforcement. This column type commonly exists in old-constructed RC frame buildings before the regulation of modern seismic codes. A stiffness-based RC frame element with shear–flexure interaction is formulated within the framework of Timoshenko beam kinematics assumption. Linked displacement interpolation functions are employed to remedy the problematic shear-locking phenomenon. The axial and flexural actions are interacted via the fiber-section model while shear-strength deterioration with inelastic flexural deformations is accounted for within the framework of the UCSD shear-strength model. The numerical procedure for shear–flexure interaction is modified from the Mergos–Kappos procedure. The proposed element is simple, computationally efficient and able to describe several salient features of RC columns with substandard detailed transverse reinforcement, including gradual spread inelasticity, shear–flexure coupling effects, and shear-strength deterioration with increasing curvature ductility. Three correlation studies are conducted to examine the model accuracy and its capability to predict the rather complex responses of non-ductile RC columns. Comparison with conventional flexural frame element is also presented to emphasize the essence of inclusion of shear response and shear–flexure interaction.

Keywords: seismic nonlinear analysis, reinforced concrete, fiber frame element, shear–flexure interaction, shear failure

1 Introduction

A large portion of old-constructed reinforced concrete (RC) frame buildings before the regulation of modern seismic codes in the mid-1970s had been severely damaged or even completely collapsed during destructive seismic events. Columns in those RC frame buildings are usually characterized by insufficient and poorly detailed transverse reinforcement (Lynn et al. 1996) and are typically referred to as “*substandard*” columns. As the most critical structural component in building systems,

column shear failure had been observed to be the main source of building damage and collapses, and represented a high risk during destructive seismic events (Moehle et al. 2001; Sezen et al. 2003). Even though some columns may have been initially designed with sectional shear capacity that sufficiently exceeds the sectional shear force induced by flexural yielding, they could eventually fail in shear due to the detrimental action of inelastic flexural deformations on the sectional shear strength (Kim et al. 2013). Several experimental evidences (e.g. Li et al. 1995; Sezen 2002) and postearthquake reconnaissance (e.g. Moehle and Mahin 1991; Sezen et al. 2003) had been observed that substandard RC columns are susceptible to shear collapse after flexural yielding. This observation stems from the fact that widening of flexural–shear cracks associated with inelastic flexural deformations

*Correspondence: suchart.l@psu.ac.th

¹ Department of Civil Engineering, Faculty of Engineering, Prince of Songkla University, Songkhla 90112, Thailand

Full list of author information is available at the end of the article

Journal information: ISSN 1976-0485 / eISSN 2234-1315

(plastic-hinge formation) impedes the concrete shear transfer mechanism driven by aggregate interlocking, thus reducing the sectional shear capacity. Several shear strength models (e.g. Priestley et al. 1993; Sezen and Moehle 2004) proposed in the research community have taken into account this detrimental effect of inelastic flexural deformations on the sectional shear capacity.

To withstand future earthquakes, seismic enhancement of substandard columns is drastically needed for old-constructed RC frame buildings. Unfortunately, rehabilitating all of these buildings to comply with current seismic regulations is a formidable task since the costs involved are extremely high. Consequently, an efficient and sufficiently accurate frame model with inclusion of shear–flexure coupling effects is required to play an essential role in assessing seismic vulnerability of existing RC frame buildings, and also in scheduling retrofitting priority in seismic rehabilitation programs.

Nowadays, it is widely accepted that nonlinear frame models have become a vital tool in seismic assessment procedures for existing RC frame buildings. However, most nonlinear frame models adopted in the standard seismic evaluation procedures for existing RC frame buildings mainly focus on inelastic flexural behaviors. Thus, development of nonlinear frame models capable of considering inelastic shear responses, detecting shear failure modes, and coupling shear with flexural actions, is still a challenging and open-ended problem.

Up to date, many researchers have proposed a variety of frame models considering inelastic shear responses. The state-of-the-art review on frame models with inclusion of shear responses was excellently presented in Ceresa et al. (2007). These models vary from relatively simple approaches in which a single shear spring is employed to represent the shear response, to frame models with sophisticated multi-dimensional constitutive laws. Pincheira et al. (1999) included shear effects into the frame element using translational springs. Though simple, this approach is only reasonable when variation of bending moment is known beforehand and the inflection point remains fixed during analysis. Filippou et al. (1992) employed a more refined approach using a subelement model in which shear deformations are considered through rotational springs at both element ends. Although this model is more accurate, shear–flexure interaction is not accounted for. Ricles et al. (1998) enhanced the one-component frame model of Giberon (1967) with stress-resultant plasticity-based end hinges. This enhanced one-component frame model could account for shear–flexure interaction and post-shear failure responses but failed to capture the gradual spreading phenomenon associated with inelastic flexural and shear responses. Mergos and Kappos (2008, 2012)

proposed a distributed flexibility model with inclusion of shear–flexure interaction. This model employed the spread plasticity and subelement concept of Soleimani (1978) and could account for several salient features of flexure–shear critical columns including gradual spread inelasticity, shear–flexure coupling effects, and shear-strength deterioration with larger curvature ductility. Nevertheless, this model requires an ad-hoc phenomenological hysteretic law for moment–curvature response and does not naturally take into account the axial–flexural interaction. In the last three decades, several finite frame elements based on fiber-section model (e.g. Limkatanyu and Spacone 2002; Panto et al. 2017) have been proposed and shown their ability to accurately predict axial and bending responses of flexure-dominated RC members. Therefore, enhancing a fiber frame model with the ability to account for shear–flexure interaction is a challenging and worth-pursuing research problem. Several researchers have attempted to incorporate shear response into the flexibility-based fiber frame model. For example; Ranzo and Petrangeli (1998) proposed a flexibility-based Timoshenko frame element in which shear and flexural actions were not interacted at the section level but were coupled through the axial-strain dependent shear strength model. Another flexibility-based Timoshenko frame element was also proposed by Marini and Spacone (2006). The flexural and shear actions in this element were not coupled at the section level as well, but were interacted through equilibrium enforcement at the element level. Though very accurate, the flexibility-based formulation usually requires a complicated element state determination procedure (Panto et al. 2017). A number of fiber frame models coupling shear and flexural actions at the section level have recently been proposed by several researchers. For example; Petrangeli et al. (1999) formulated a flexibility-based Timoshenko frame model with the ability to capture shear response and shear–flexure interaction at the section level, accomplished using the microplane model (Ozbolt and Bazant 1992). Ceresa et al. (2009) formulated a stiffness-based Timoshenko frame element in which shear and flexure actions was interacted at the section level using the Modified Compression Field Theory (MCFT) developed by Palermo and Vecchio (2003). Kagermanov and Ceresa (2017) enhanced the flexibility-based frame element of Spacone et al. (1996) with an exact shear strain profile. This novel fiber-section model was developed based on a smeared-crack/fixed crack membrane model by Kagermanov and Ceresa (2016) and allowed for the shear–flexure interaction at the section level. Even though these frame models are very accurate and take into account the sectional shear–flexure interaction in a very precise manner, sophisticated multi-dimensional constitutive laws and

high implementation efforts are usually required. These could prohibit the model usage by practicing structural engineers, and the computational costs involved are usually high.

In light of the above discussion, there is still room to propose an additional frame model for the research and practicing-engineer communities. Consequently, the present work is aimed at proposing an improved finite frame element with shear–flexure interaction. This proposed model needs to be simple but sufficiently accurate and capable of being programmed into a general-purpose finite element platform with ease. Furthermore, the model inputs need to be closely related to actual engineering properties to render the proposed model accessible by an even wider range of practicing structural engineers and researchers.

Organization of the present work is as following outlined. Equilibrium, compatibility, and sectional constitutive relations of the Timoshenko frame model are first derived. Stiffness-based framework of the model formulation is presented next. The virtual displacement principle is at the core of the model formulation and the resulting model can be programmed with ease. To remedy the problematic shear locking phenomenon, linked displacement interpolation functions are employed, thus resulting in the locking-free Timoshenko frame element. Subsequently, the shear–flexure interaction procedure is discussed. The present study adopts and modifies the interaction procedure proposed by Mergos and Kappos (2008, 2012) within the framework of the so-called “UCSD Shear-Strength Model” proposed by Priestley et al. (1993). Finally, three correlation studies are conducted to examine the model accuracy and its ability to represent the rather complex responses of non-ductile RC columns. The first two correlation studies focus on flexure–shear critical columns while the third emphasizes on a shear-dominated column. The finite element platform FEAP (Taylor 2000) is used to host the proposed frame element.

2 Governing Equations of Timoshenko Frame Element

2.1 Equilibrium Relations

An infinitesimal segment dx taken from a frame member under transverse load $p_y(x)$ is shown in Fig. 1. Considering axial, moment, and vertical equilibriums of this segment yields the following relations:

$$\frac{dN(x)}{dx} = 0 \tag{1}$$

$$\frac{dM(x)}{dx} + V(x) = 0 \tag{2}$$

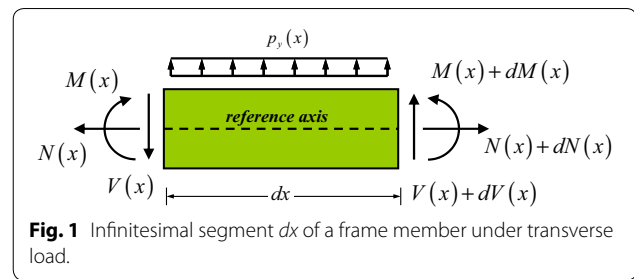


Fig. 1 Infinitesimal segment dx of a frame member under transverse load.

$$\frac{dV(x)}{dx} + p_y(x) = 0 \tag{3}$$

where $N(x)$ is the frame sectional axial force; $V(x)$, the frame sectional shear force; and $M(x)$, the frame sectional bending moment.

The matrix form of Eqs. (1) (2), and (3) can be expressed as:

$$\mathbf{L}_{TB}^T \mathbf{D}(x) - \mathbf{p}(x) = \mathbf{0} \tag{4}$$

where $\mathbf{D}(x) = \{ N(x) \ M(x) \ V(x) \}^T$ represents the element sectional force vector; $\mathbf{p}(x) = \{ 0 \ 0 \ p_y(x) \}^T$, the element distributed load vector; and \mathbf{L}_{TB} , the differential operator, given as:

$$\mathbf{L}_{TB} = \begin{bmatrix} \frac{d}{dx} & 0 & 0 \\ 0 & \frac{d}{dx} & 0 \\ 0 & 1 & -\frac{d}{dx} \end{bmatrix} \tag{5}$$

2.2 Compatibility Relations

As work conjugate of the element sectional force vector $\mathbf{D}(x)$, the element sectional deformation vector $\mathbf{d}(x)$ is defined as:

$$\mathbf{d}(x) = \{ \varepsilon_0(x) \ \varphi(x) \ \gamma(x) \}^T \tag{6}$$

where $\varepsilon_0(x)$ is the sectional axial strain at reference axis; $\varphi(x)$, the sectional bending curvature; and $\gamma(x)$, the sectional shear strain.

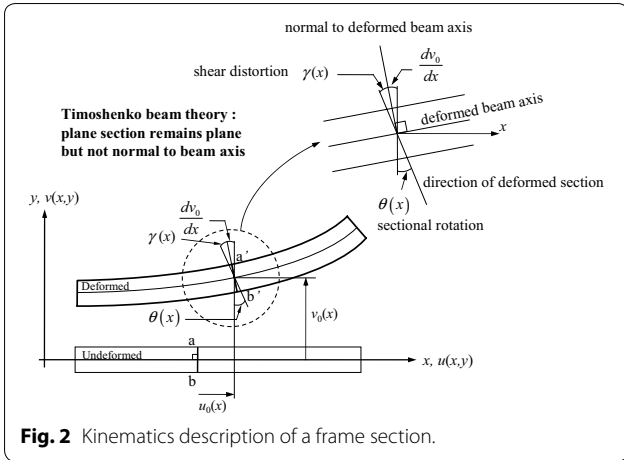
At the element level, the following sectional displacements are collected in a vector form as:

$$\mathbf{u}(x) = \{ u_0(x) \ \theta(x) \ v_0(x) \}^T \tag{7}$$

where $u_0(x)$ is the sectional axial displacement at reference axis; $\theta(x)$, the sectional rotation; and $v_0(x)$, the sectional transverse displacement.

Figure 2 depicts kinematics description of the frame section following the Timoshenko beam hypothesis.

Through the compatibility conditions, element sectional deformations are related to the element sectional displacements as:



$$\varepsilon_0(x) = \frac{du_0(x)}{dx} \tag{8}$$

$$\varphi(x) = \frac{d\theta(x)}{dx} \tag{9}$$

$$\gamma(x) = \theta(x) - \frac{dv_0(x)}{dx} \tag{10}$$

and can be written together in the matrix form as:

$$\mathbf{d}(x) = \mathbf{L}_{TB} \mathbf{u}(x) \tag{11}$$

2.3 Sectional Force–Deformation Relations

In this work, the nonlinear feature of RC responses is entirely based on a nonlinear deformation-based constitutive model, defined as:

$$\mathbf{D}(x) = \Psi[\mathbf{d}(x)] \tag{12}$$

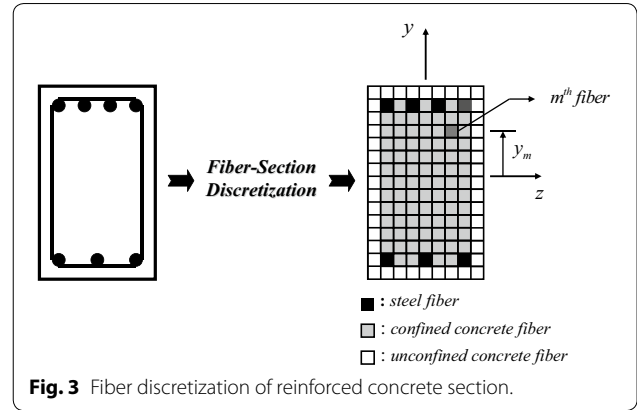
Equation (13) expresses the linearized incremental form of Eq. (12) as:

$$\mathbf{D}(x) = \mathbf{D}^0(x) + \mathbf{k}^0(x) \Delta \mathbf{d}(x) \tag{13}$$

where $\mathbf{D}^0(x)$ and $\mathbf{k}^0(x)$ are the sectional force vector and the stiffness matrix at the initial point, respectively. Superscript 0 indicates the value of a vector or matrix at the initial point of the incremental-iterative solution procedure.

In this study, the fiber-section model is employed to derive the incremental relation of Eq. (13). The fiber-section model can automatically account for the axial–flexural interaction (Spacone and Limkatanyu 2000). Figure 3 shows the fiber-section discretization. The sectional axial force $N(x)$ and sectional moment $M(x)$ are defined as:

$$N(x) = \sum_{m=1}^{nfib} \sigma_m A_m \quad \text{and} \quad M(x) = - \sum_{m=1}^{nfib} y_m \sigma_m A_m \tag{14}$$



where m defines the generic fiber, and $nfib$ represents the number of fibers in the section; y_m , σ_m , and A_m represent the distance from the reference axis x (Fig. 3), the normal stress, and the area, respectively, of the m th fiber in the section.

With Eq. (14), the element sectional force vector $\mathbf{D}(x)$ can be rewritten as:

$$\mathbf{D}(x) = \left\{ \begin{matrix} \sum_{m=1}^{nfib} \sigma_m A_m & - \sum_{m=1}^{nfib} y_m \sigma_m A_m & V(x) \end{matrix} \right\}^T \tag{15}$$

It is worth observing from Eq. (15) that $nfib$ fibers are required in section discretization to represent the axial and bending actions due to variation of the normal stress σ_m along the section depth, while there is no need for fiber-section discretization to represent the shear action due to the constant shear stress along the section depth following the Timoshenko beam theory (Onate 2013). In other words, the fiber-section discretization for shear action is analogous to the one-fiber discretization.

The sectional stiffness matrix $\mathbf{k}(x)$ can be expressed via the fiber-section model as:

$$\mathbf{k}(x) = \begin{bmatrix} \sum_{m=1}^{nfib} E_m A_m & - \sum_{m=1}^{nfib} y_m E_m A_m & 0 \\ - \sum_{m=1}^{nfib} y_m E_m A_m & \sum_{m=1}^{nfib} y_m^2 E_m A_m & 0 \\ 0 & 0 & GA_s(x) \end{bmatrix} \tag{16}$$

where E_m is the modulus of the m th fiber in the section; and $GA_s(x)$ is the sectional shear stiffness.

From Eq. (16), there is no coupling between shear and flexural actions. However, interaction between these two effects can be triggered via the shear strength model employed in this study, and will be discussed later in the paper.

Uniaxial cyclic constitutive laws employed in this study for concrete, reinforcing steel, and shear responses are schematically shown in Fig. 4 to ease model implementation. Kent and Park (1971) law is used for concrete response; Menegotto and Pinto (1973) law is used for reinforcing steel response; and the tri-linear envelope curve proposed by Mergos and Kappos (2012) is used for shear response.

3 Stiffness-Based Formulation of Timoshenko Frame Element

3.1 Formulation

In this work, the proposed element is constructed with the stiffness-based finite element formulation. Through appropriate interpolation functions, element sectional displacements $\mathbf{u}(x)$ can be expressed in terms of the element nodal displacements \mathbf{U} . Element deformations $\mathbf{d}(x)$ are obtained by enforcing the section compatibility of Eq. (11).

Equation (17) defines the weighted residual expression of Eq. (4) as:

$$\int_L \delta \mathbf{u}^T(x) \left[\mathbf{L}_{TB}^T \mathbf{D}(x) - \mathbf{p}(x) \right] dx = 0 \tag{17}$$

with $\delta \mathbf{u}(x)$ being a vector containing compatible virtual displacement fields.

Substituting Eq. (13) into (17) and enforcing compatibility of Eq. (11) lead to:

$$\int_L \delta \mathbf{u}^T(x) \left[\mathbf{L}_{TB}^T \left(\mathbf{D}^0(x) + \mathbf{k}^0(x) \mathbf{L}_{TB} \Delta \mathbf{u}(x) \right) - \mathbf{p}(x) \right] dx = 0 \tag{18}$$

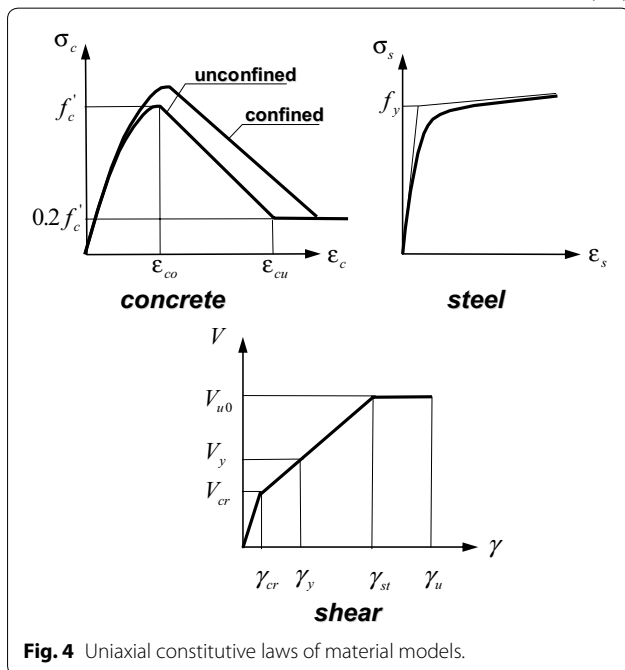


Fig. 4 Uniaxial constitutive laws of material models.

Integration by parts is applied to Eq. (18), thus resulting in:

$$\begin{aligned} & \int_L (\mathbf{L}_{TB} \delta \mathbf{u}(x))^T \mathbf{k}^0(x) (\mathbf{L}_{TB} \Delta \mathbf{u}(x)) dx \\ &= \delta \mathbf{U}^T \mathbf{P} + \int_L \delta \mathbf{u}^T(x) \mathbf{p}(x) dx - \int_L (\mathbf{L}_{TB} \delta \mathbf{u}(x))^T \mathbf{D}^0(x) dx \end{aligned} \tag{19}$$

where $\delta \mathbf{U}^T \mathbf{P}$ defines the external virtual work done and is obtained from the boundary terms during integration by parts.

Through the displacement interpolation function matrix $\mathbf{N}_{TB}(x)$, the element sectional displacements $\mathbf{u}(x)$ are expressed in terms of the element nodal displacements \mathbf{U} as:

$$\mathbf{u}(x) = \mathbf{N}_{TB}(x) \mathbf{U} \tag{20}$$

For the Timoshenko frame element, the selection of displacement interpolation functions must be made with care and is to be discussed in the subsequent section. Substituting Eq. (20) into (19) and accounting for the arbitrariness of $\delta \mathbf{U}$ lead to:

$$\begin{aligned} & \left[\int_L \mathbf{B}_{TB}(x)^T \mathbf{k}^0(x) \mathbf{B}_{TB}(x) dx \right] \Delta \mathbf{U} \\ &= \mathbf{P} + \int_L \mathbf{N}_{TB}(x)^T \mathbf{p}(x) dx - \int_L \mathbf{B}_{TB}(x)^T \mathbf{D}^0(x) dx \end{aligned} \tag{21}$$

where $\mathbf{B}_{TB}(x) = \mathbf{L}_{TB} \mathbf{N}_{TB}(x)$ is the sectional deformation-displacement matrix.

The matrix form of Eq. (21) is:

$$\mathbf{K}^0 \Delta \mathbf{U} = (\mathbf{P} + \mathbf{P}_p) - \mathbf{Q}^0 \tag{22}$$

where $\mathbf{K}^0 = \int_L \mathbf{B}_{TB}(x)^T \mathbf{k}^0(x) \mathbf{B}_{TB}(x) dx$ is the frame element stiffness matrix; $\mathbf{P}_p = \int_L \mathbf{N}_{TB}(x)^T \mathbf{p}(x) dx$ is the equivalent load vector due to the distributed load $\mathbf{p}(x)$; $\mathbf{Q}^0 = \int_L \mathbf{B}_{TB}(x)^T \mathbf{D}^0(x) dx$ is the element resisting force vector.

Equation (22) represents the incremental form of the element stiffness equation and the term on its right-hand side defines the residual force vector associated with the weak statement of equilibrium equations. Once equilibrium configuration is reached during the incremental-iterative solution procedure, this residual force vector vanishes.

3.2 Linked Displacement Interpolation Functions

In Timoshenko beam theory, the sectional rotation field $\theta(x)$ is independent of the sectional transverse displacement field $v_0(x)$. Consequently, the sectional rotation

$\theta(x)$ and sectional transverse displacement $v_0(x)$ can be interpolated independently to their nodal values in the stiffness-based formulation of Timoshenko frame model. Nevertheless, inattentive selection of independent interpolation functions for the sectional transverse displacement $v_0(x)$ and sectional rotation $\theta(x)$ fields may cause the resulting Timoshenko frame model to suffer from the problematic phenomenon known as “shear locking”. Diagnosis of the shear-locking phenomenon is thoroughly discussed in Onate (2013).

In this study, the consistent interpolation approach is employed to overcome the shear-locking problem. This approach requires that the choice of interpolation functions for the sectional transverse displacement $v_0(x)$ and the sectional rotation $\theta(x)$ fields has to be such that $dv_0(x)/dx$ and $\theta(x)$ are polynomials of the same order. In other words, the interpolation function for the sectional transverse displacement field $v_0(x)$ must be one-degree higher than that for the sectional rotation field $\theta(x)$. Consequently, a standard linear Timoshenko frame element, shown in Fig. 5, is to be enhanced with a quadratic (bubble) term for the sectional transverse displacement field $v_0(x)$. The resulting interpolation functions are:

$$u_0(x) = \left(1 - \frac{x}{L}\right)U_1 + \frac{x}{L}U_4 \tag{23}$$

$$v_0(x) = \left(1 - \frac{x}{L}\right)U_2 + \frac{x}{L}U_5 + \underbrace{\alpha x(x-L)}_{\text{Enhanced Bubble Function (24)}} \tag{24}$$

$$\theta(x) = \left(1 - \frac{x}{L}\right)U_3 + \frac{x}{L}U_6 \tag{25}$$

with $\mathbf{U} = \{U_1 \ U_2 \ U_3 \ U_4 \ U_5 \ U_6\}^T$ being a vector collecting element nodal displacements, and α is a parameter to be determined from the limit Euler–Bernoulli condition of vanishing shear strain ($\gamma = 0$) for slender beams.

Based on Eqs. (10), (24), and (25), the sectional shear strain can be expressed as:

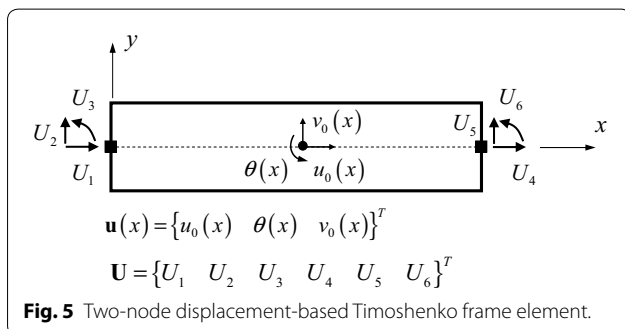


Fig. 5 Two-node displacement-based Timoshenko frame element.

$$\gamma(x) = \left(\frac{U_2 - U_5}{L}\right) + U_3 + \alpha L + x\left(\frac{U_6 - U_3}{L} - 2\alpha\right) \tag{26}$$

To ensure the condition of vanishing shear strain ($\gamma = 0$) for slender beams within the limit, Eq. (26) must be independent of the coordinate x , thus leading to the following relation:

$$\alpha = \frac{U_6 - U_3}{2L} \tag{27}$$

Combining Eq. (24) and Eq. (27) yields the expression for the enhanced sectional transverse displacement field $v_0(x)$ as:

$$v_0(x) = \left(1 - \frac{x}{L}\right)U_2 + \frac{x}{L}U_5 + \left(\frac{x}{2} - \frac{x^2}{2L}\right)U_3 + \left(-\frac{x}{2} + \frac{x^2}{2L}\right)U_6 \tag{28}$$

Equation (28) clearly indicates that the sectional transverse displacement field $v_0(x)$ is interpolated not only in terms of nodal displacements (U_2 and U_5) but also in terms of nodal rotations (U_3 and U_6), thus leading to the so-called “linked” displacement interpolation functions (Fraeijs de Veubeke 1965).

Based on Eqs. (23), (25), and (28), the displacement interpolation function matrix $\mathbf{N}_{TB}(x)$ is:

$$\mathbf{N}_{TB}(x) = \begin{bmatrix} 1 - \frac{x}{L} & 0 & 0 & \frac{x}{L} & 0 & 0 \\ 0 & 0 & 1 - \frac{x}{L} & 0 & 0 & \frac{x}{L} \\ 0 & 1 - \frac{x}{L} & \frac{x}{2} - \frac{x^2}{2L} & 0 & \frac{x}{L} & -\frac{x}{2} + \frac{x^2}{2L} \end{bmatrix} \tag{29}$$

The sectional deformation-displacement matrix $\mathbf{B}_{TB}(x)$ is:

$$\mathbf{B}_{TB}(x) = \mathbf{L}_{TB}\mathbf{N}_{TB}(x) = \begin{bmatrix} -\frac{1}{L} & 0 & 0 & \frac{1}{L} & 0 & 0 \\ 0 & 0 & -\frac{1}{L} & 0 & 0 & \frac{1}{L} \\ 0 & \frac{1}{L} & \frac{1}{2} & 0 & -\frac{1}{L} & \frac{1}{2} \end{bmatrix} \tag{30}$$

4 UCSD Shear Strength Model

Among several shear-strength models proposed in the research community, the so-called “UCSD Shear-Strength Model” presented by Priestley et al. (1993) is adopted herein because of its validity and capability. The UCSD shear-strength model has an ability to consider the shear strength deterioration with increasing curvature ductility demand. This feature is very attractive and is suited to the development of RC frame element considering shear–flexure interaction effects in this work.

In the UCSD shear-strength model, there are three resisting mechanisms contributing to the shear strength V_u , namely: concrete mechanism V_c ; truss mechanism (transverse reinforcement) V_s ; and arch mechanism (axial force) V_a .

$$V_u = V_c + V_s + V_a \tag{31}$$

The concrete shear strength V_c is defined as:

$$V_c = k_\phi \sqrt{f'_c} (0.8A_g) \tag{32}$$

where f'_c is the concrete compressive cylinder strength (in MPa); A_g , the gross cross sectional area; and k_ϕ , a coefficient considering the influence of curvature ductility μ_ϕ on concrete shear strength V_c as shown in Fig. 6.

For a rectangular section, the transverse-reinforcement shear strength V_s associated with the truss mechanism (Park and Paulay 1975) is defined as:

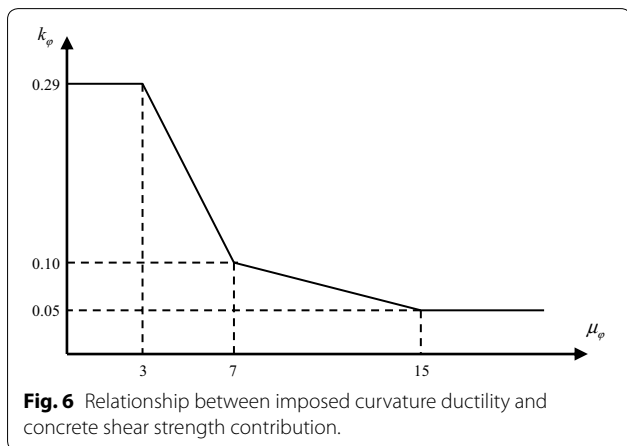
$$V_s = \frac{A_v f_{yv} D'}{s} \cot 30^\circ \tag{33}$$

where s is the spacing of transverse reinforcement measured parallel to the longitudinal reinforcement; A_v , the transverse reinforcement area with spacing s ; f_{yv} , the yield strength of transverse reinforcement; and D' , the distance measured parallel to the applied shear between centers of the longitudinal reinforcement.

The axial-force shear strength V_a associated with the arch mechanism is expressed as:

$$V_a = N \tan \beta \tag{34}$$

where N is the compressive axial force, and β is the angle between the column axis and the line connecting the centers of the flexural compression zones at the top and the bottom of the column ends. The axial-force shear strength V_a is not degraded with increasing ductility as pointed out by Priestley et al. (1993).



5 Sectional Shear Constitutive Model

5.1 Undamaged Primary Curve

For sectional shear response, the envelope curve proposed by Mergos and Kappos (2008, 2012) is adopted to define the undamaged primary curve. There are four linear portions with three different slopes defined on the undamaged primary curve of Fig. 7.

The first linear portion oa with uncracked slope $(GA)_0$ represents the elastic behavior of uncracked section in shear, and connects the origin point o to the cracking point a (V_{cr} , γ_{cr}) at which the nominal principal tensile stress becomes larger than the nominal tensile strength of concrete. The cracking shear force V_{cr} and the uncracked slope $(GA)_0$ are suggested by Sezen and Moehle (2004) as:

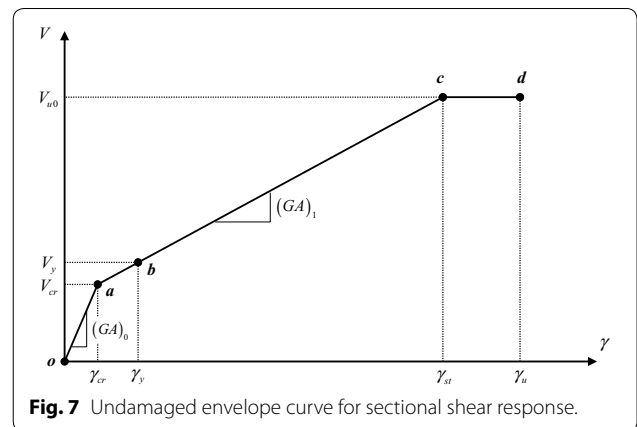
$$V_{cr} = \left(\frac{f'_t}{(L_a/h)} \sqrt{\left(1 + \frac{N}{f'_t A_g} \right)} \right) 0.80A_g \tag{35}$$

and $(GA)_0 = 0.80 GA_g$

where f'_t is the nominal tensile strength of concrete; G , the concrete shear modulus; and L_a/h , the shear span ratio. The cracking shear strain is simply defined as:

$$\gamma_{cr} = \frac{V_{cr}}{(GA)_0} \tag{36}$$

The second linear ab and the third linear bc portions have the same slope as $(GA)_1$. The second linear portion ab connects the cracking point a (V_{cr} , γ_{cr}) to the flexural-yielding point b (V_y , γ_y) at which the longitudinal reinforcement experiences a yielding state for the first time. The yielding information of the longitudinal reinforcement is provided by the fiber-section model. The third linear portion bc links the flexural-yielding point b (V_y , γ_y) to the point c (V_{u0} , γ_{st}) at which the shear force reaches its ultimate value V_{u0} while the shear strain γ_{st} corresponds to the verge of transverse reinforcement yielding. Traditionally, the value of shear strain γ_{st} can simply be computed



based on the truss analogy (Park and Paulay 1975). However, Mergos and Kappos (2008, 2012) recognized that values of shear strain γ_{st} based on the truss analogy did not correspond well with experimental results since the effects of axial load and member aspect ratio on the shear strain γ_{st} were not considered in the truss analogy approach. To account for these two effects, Mergos and Kappos (2012) recommended the following two correction parameters κ and γ based on regression analyses and proposed the new expression for the shear strain γ_{st} as:

$$\gamma_{st} = \kappa \lambda \gamma_{truss} \tag{37}$$

where $\kappa = 1 - 1.07 \left(\frac{N}{f_c A_g} \right)$ is the axial-force correction parameter; $\lambda = 5.37 - 1.59 \min \left(2.5, \frac{L_a}{h} \right)$, the member-aspect-ratio correction parameter; and γ_{truss} , the shear strain associated with the yielding of transverse reinforcement based on the truss analogy approach (Park and Paulay 1975), and can be expressed as:

$$\gamma_{truss} = \frac{V_{cr}}{(GA)_0} + \frac{A_v f_{yv} \left(\sin^4 \phi + \frac{E_s}{E_c} \rho_w \right)}{s E_s b \rho_w \sin^4 \phi \cot \phi} \tag{38}$$

where E_s is the steel modulus of elasticity; E_c , the concrete modulus of elasticity; b , the section width; ρ_w , the volumetric ratio of transverse reinforcement; and ϕ , the angle characterized by the member axis and the direction of diagonal struts. Mergos and Kappos (2012) performed regression analyses between experimental and analytical results and recommended that angle ϕ of 45° is the optimal value.

The flat-top portion cd characterizing plastic behavior of shear response connects the shear-yielding point c (V_{u0} , γ_{st}) to the ultimate point d (V_{u0} , γ_u) at which the shear strain reaches its ultimate value γ_u . This flat-top portion corresponds to the experimental observation that shear-critical reinforced concrete members can experience additional shear deformation under sustained shear force before the onset of shear failure (Ma et al. 1976; Aboutaha et al. 1999). Consequently, the shear strain γ_u associated with the onset of shear failure (significant strength deterioration) could be considerably larger than the shear strain γ_{st} (Gerin and Adebar 2004; Sezen 2008; Mergos and Kappos 2012). Based on regression analyses of experimental results for 25 RC members eventually failing in shear, Mergos and Kappos (2012) proposed the following expression for the ultimate shear strain γ_u :

$$\gamma_u = \lambda_1 \lambda_2 \lambda_3 \gamma_{st} \geq \gamma_{st} \tag{39}$$

where $\lambda_1 = 1 - 2.5 \min \left(0.4, \frac{N}{f_c A_g} \right)$ is the parameter accounting for the axial load; $\lambda_2 = \min \left(2.5, \frac{L_a}{h} \right)^2$ is the parameter accounting for the member aspect ratio; and

$\lambda_3 = 0.31 + 17.8 \min \left(\frac{A_v f_{yv}}{b s f_c}, 0.08 \right)$ is the parameter accounting for the amount of transverse reinforcement.

5.2 Modified Mergos–Kappos Shear–Flexure Interaction Procedure

Adverse influences of inelastic flexural deformation on shear resistance have long been recognized in the research community. Several researchers have noticed and demonstrated that shear strength of an RC section in the plastic hinge region decreases with increasing inelastic flexural deformation (Ghee et al. 1989; Priestley et al. 1993; Sezen 2002). This shear-strength deterioration is caused by concrete disintegration associated with inelastic flexural deformation (plastic-hinge formation). Moreover, several experimental results (e.g. Lynn 2001; Sezen 2002) indicate that sectional shear strain in the plastic hinge region increases drastically following formation of the plastic hinge despite approximately constant shear force confined by the flexural yielding. These two phenomena result from interaction between the shear and flexural actions and can be considered together by integrating the UCSD shear-strength model with the truss analogy approach as suggested by Mergos and Kappos (2008, 2012).

This study adopts and modifies the shear–flexure interaction procedure suggested by Mergos and Kappos (2008, 2012). Figure 8 shows the general scheme for the shear–flexure interaction procedure and the evolution of the reduced shear envelope curve with increasing curvature ductility. Degradation in the shear strength is associated with reduction in the concrete shear-strength contribution V_c as dictated by the UCSD shear-strength model, and is accounted for by reducing the ordinate of the undamaged shear envelope. The sectional shear response starts to deviate from the undamaged envelope curve when there is degradation in the shear strength. The damaged (reduced) shear envelope curve keeps on updating with evolution of the reduced shear strength and the resulting envelope curve is along the path $o - a - b - e - f' - g' - h' - c^g - d^g$. Figure 8 shows that there are three cases encountered when the shear–flexure interaction is triggered once yielding of flexural reinforcement takes place at point b . General representation of the shear–flexure interaction procedure adopted herein is depicted in Fig. 9 for all cases.

In Case I, shown in Fig. 9a, the sectional curvature ductility does not attain the value of 3. Consequently, there is no strength degradation in shear following the UCSD shear-strength model (Fig. 6). In this case, sectional shear response points at the start and the end of the load increment step both lie on the undamaged shear envelop with the cracked sectional shear stiffness $(GA)_1$.

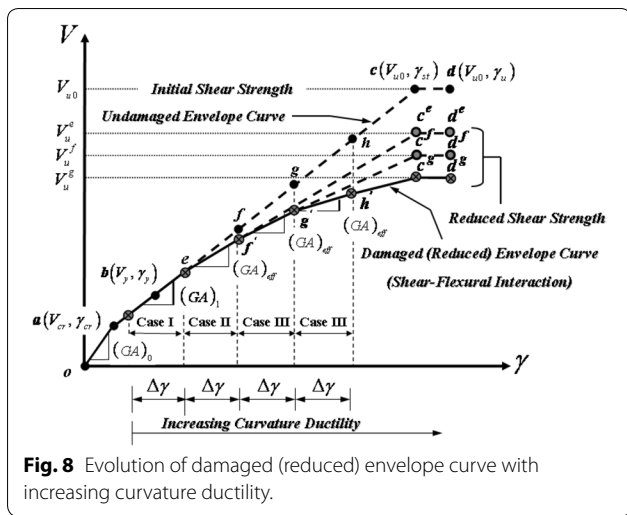


Fig. 8 Evolution of damaged (reduced) envelope curve with increasing curvature ductility.

In Case II, shown in Fig. 9b, the sectional curvature ductility exceeds the value of 3 for the first time. As a result, there is strength degradation in shear based on the UCSD shear-strength model (Fig. 6). In this case, the sectional shear response point at the start of the load increment step lies on the undamaged shear envelop while the sectional shear response point at the end of the load increment step is on the damaged (reduced) shear envelop with the effective sectional shear stiffness $(GA)_{eff}$.

In Case III, shown in Fig. 9c, the sectional shear response points at the start and the end of the load increment step both lie on the damaged shear envelop with the effective sectional shear stiffness $(GA)_{eff}$.

In the present work, the shear–flexure interaction procedure originally proposed by Mergos and Kappos (2008, 2012) is modified to compute the incremental sectional shear force ΔV and the effective sectional shear stiffness

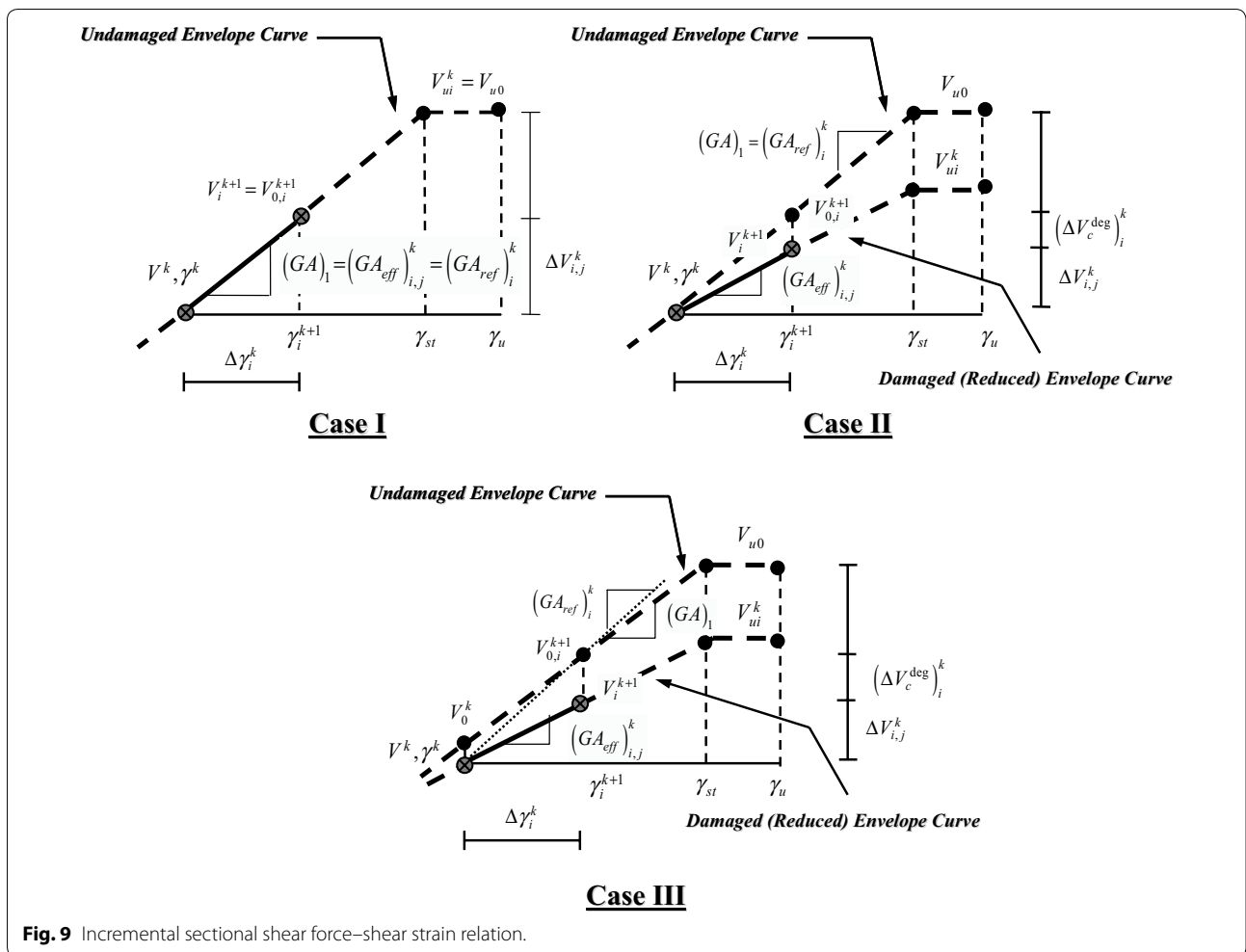


Fig. 9 Incremental sectional shear force–shear strain relation.

$(GA)_{eff}$ for a given incremental sectional shear strain $\Delta\gamma$ for all above-mentioned cases. Consequently, the authors will refer to the employed procedure as the “*modified Mergos–Kappos*” shear–flexure interaction procedure.

In this procedure, the so-called reference shear stiffness $(GA_{ref})_i^k$ is defined as:

$$(GA_{ref})_i^k = \frac{V_{0,i}^{k+1} - V^k}{\Delta\gamma_i^k} \tag{40}$$

where $V_{0,i}^{k+1}$ is the non-degraded sectional shear force corresponding to the sectional shear strain $\gamma_i^{k+1} = \gamma^k + \Delta\gamma_i^k$ and can be defined as:

$$V_{0,i}^{k+1} = V_{cr} + (GA)_1(\gamma_i^{k+1} - \gamma_{cr}) \tag{41}$$

It is noted that in Cases I and II, the reference sectional shear stiffness $(GA_{ref})_i^k$ is simply equal to the cracked sectional shear stiffness $(GA)_1$ as shown in Fig. 9a, b. Considering the geometric relation in Fig. 9 leads to the following expression:

$$\Delta\gamma_i^k = \frac{\Delta V_i^k}{(GA_{eff})_i^k} = \frac{\Delta V_i^k + (\Delta V_c^{deg})_i^k}{(GA_{ref})_i^k} \tag{42}$$

where ΔV_i^k is the incremental sectional shear force, and $(\Delta V_c^{deg})_i^k$ is the reduction in sectional shear force associated with the concrete shear strength degradation and can be defined as:

$$(\Delta V_c^{deg})_i^k = (GA_{ref})_i^k \Delta\gamma_i^k - \left(\frac{V_{ui}^k - V^k}{\gamma_{st} - \gamma^k} \right) \Delta\gamma_i^k \tag{43}$$

where V_{ui}^k is the reduced shear strength dictated by variation of the concrete-contribution coefficient k_φ with sectional curvature ductility μ_φ (Fig. 6).

Based on Eq. (42), relation between the effective sectional shear stiffness $(GA_{eff})_i^k$ and the reference sectional shear stiffness $(GA_{ref})_i^k$ can be established as:

$$(GA_{eff})_i^k = \frac{\Delta V_i^k}{\Delta V_i^k + (\Delta V_c^{deg})_i^k} (GA_{ref})_i^k \tag{44}$$

It is observed from Eqs. (42) and (44) that the effective sectional shear stiffness $(GA_{eff})_i^k$ and the incremental sectional shear force ΔV_i^k are mutually dependent. To obtain these two quantities, an additional iterative procedure is required within the element iterative step i of the load increment k . It is worth remarking that the following

quantities $(GA_{ref})_i^k$, $(\Delta V_c^{deg})_i^k$, and $\Delta\gamma_i^k$ are unchanged during this additional iterative process. An additional subscript “ j ” is appended to $(GA_{eff})_i^k$ and ΔV_i^k to indicate the iterative step within the shear–flexure interaction procedure.

Based on Eqs. (42) and (44), the residual function $\Phi((GA_{eff})_{ij}^k)$ can be defined as:

$$\Phi((GA_{eff})_{ij}^k) = (GA_{eff})_{ij}^k \Delta\gamma_i^k - \frac{(GA_{eff})_{ij}^k (\Delta V_c^{deg})_i^k}{(GA_{ref})_i^k - (GA_{eff})_{ij}^k} \tag{45}$$

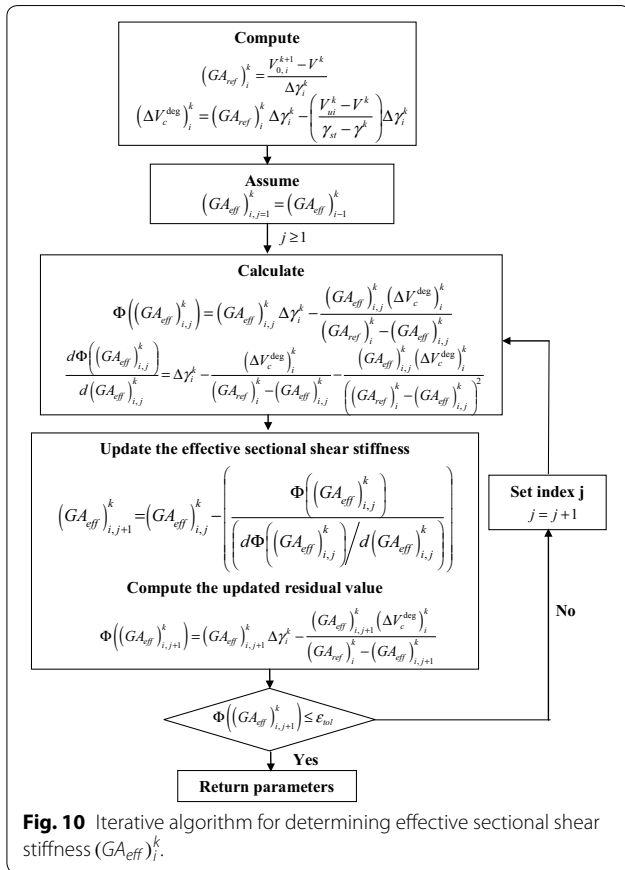
The Newton–Raphson method is to be employed to solve for the solution to Eq. (45). The derivative of Eq. (45) with respect to $(GA_{eff})_{ij}^k$ is:

$$\frac{d\Phi((GA_{eff})_{ij}^k)}{d(GA_{eff})_{ij}^k} = \Delta\gamma_i^k - \frac{(\Delta V_c^{deg})_i^k}{(GA_{ref})_i^k - (GA_{eff})_{ij}^k} - \frac{(GA_{eff})_{ij}^k (\Delta V_c^{deg})_i^k}{((GA_{ref})_i^k - (GA_{eff})_{ij}^k)^2} \tag{46}$$

The step-by-step algorithm shown in Fig. 10 for the Newton–Raphson iterative procedure within the shear–flexure interaction procedure is as follows:

1. Compute the reference sectional shear stiffness $(GA_{ref})_i^k$ from Eq. (40), and the reduction in sectional shear force associated with the concrete shear strength degradation $(\Delta V_c^{deg})_i^k$ from Eq. (43).
2. Assume an initial value of $(GA_{eff})_{i,j=1}^k$. In this study, it is suggested to set $(GA_{eff})_{i,j=1}^k = (GA_{eff})_{i-1}^k$.
3. Start the iterative procedure ($j \geq 1$) for the shear–flexure interaction within the element iterative step i of the load increment k ,
 - a. Compute the residual function $\Phi((GA_{eff})_{ij}^k)$ based on Eq. (45):

$$\Phi((GA_{eff})_{ij}^k) = (GA_{eff})_{ij}^k \Delta\gamma_i^k - \frac{(GA_{eff})_{ij}^k (\Delta V_c^{deg})_i^k}{(GA_{ref})_i^k - (GA_{eff})_{ij}^k}$$



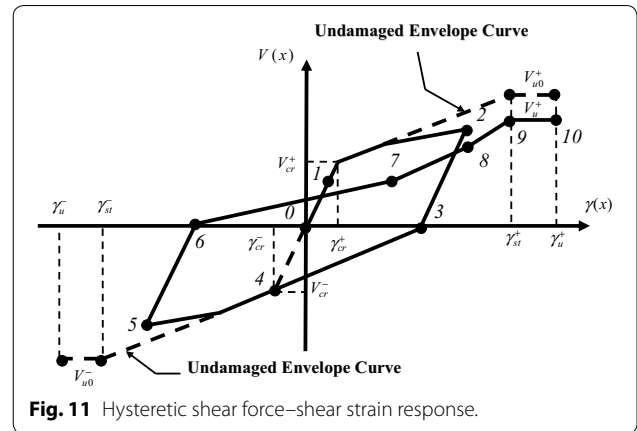
- b. Compute the slope $d\Phi((GA_{eff})_{ij}^k)/d(GA_{eff})_{ij}^k$ based on Eq. (46):

$$\frac{d\Phi((GA_{eff})_{ij}^k)}{d(GA_{eff})_{ij}^k} = \Delta\gamma_i^k - \frac{(\Delta V_c^{deg})_i^k}{(GA_{ref})_i^k - (GA_{eff})_{ij}^k} - \frac{(GA_{eff})_{ij}^k (\Delta V_c^{deg})_i^k}{((GA_{ref})_i^k - (GA_{eff})_{ij}^k)^2}$$

- c. Update the effective sectional shear stiffness $(GA_{eff})_{i,j+1}^k$:

$$(GA_{eff})_{i,j+1}^k = (GA_{eff})_{ij}^k - \left(\frac{\Phi((GA_{eff})_{ij}^k)}{d\Phi((GA_{eff})_{ij}^k)/d(GA_{eff})_{ij}^k} \right)$$

- d. Compute the updated residual value $\Phi((GA_{eff})_{i,j+1}^k)$

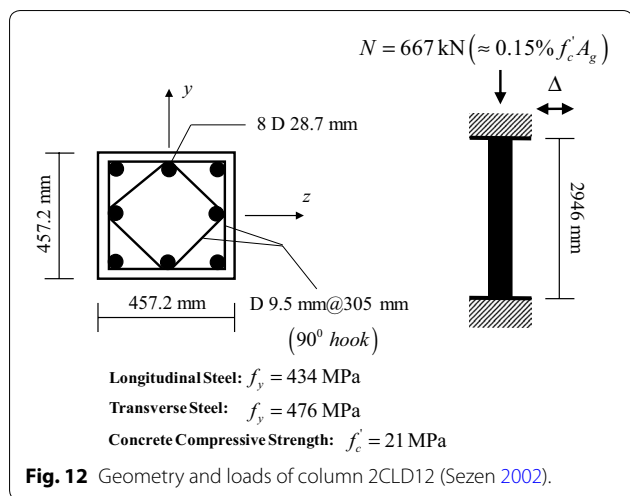


4. Check if the updated residual value in step 3(d) is less than the convergence tolerance ϵ_{tol} :
- i. If no, set $j = j + 1$ and return to step 3(a).
 - ii. If yes, return the current sectional shear force $V_i^{k+1} = V_i^k + (GA_{eff})_{ij}^k \Delta\gamma_i^k$ and the current effective sectional shear stiffness $(GA_{eff})_{ij}^k$

5.3 Hysteretic Shear Force–Shear Strain Response

To describe the sectional shear response under cyclic loading, a hysteretic model is required. In this work, a general hysteretic model presented by Filippou et al. (1992) and later enhanced by Martino (1999) is adopted and modified to describe the sectional shear force–deformation response under cyclic load reversals. This hysteretic model is attractive since it can represent both the damage and the pinching effects associated with shear crack closing and opening. The general shape of the modified hysteretic shear model is shown in Fig. 11 and its general feature of the hysteresis law can be briefly described as follows:

The section is loaded first along the monotonic branch 0-1-2 and then is unloaded along the path 2-3 with the initial stiffness $(GA)_0$ until it reaches the abscissa at point 3. As unloading is reloading, and reloading continues in the opposite direction along the path 3-4-5, the section experiences a crack closing process until it reaches the monotonic envelope on the opposite side at point 4 and continues loading along the path 4-5. At point 5, the section is unloaded along the path 5-6 and starts to reload in the opposite direction along the path 6-7-8 on which the section experiences the crack closing process, thus resulting in the pinching response. Along the path 8-9-10, the section response travels along the reduced envelope. More details on the



hysteresis law can be found in Filippou et al. (1992) and Martino (1999).

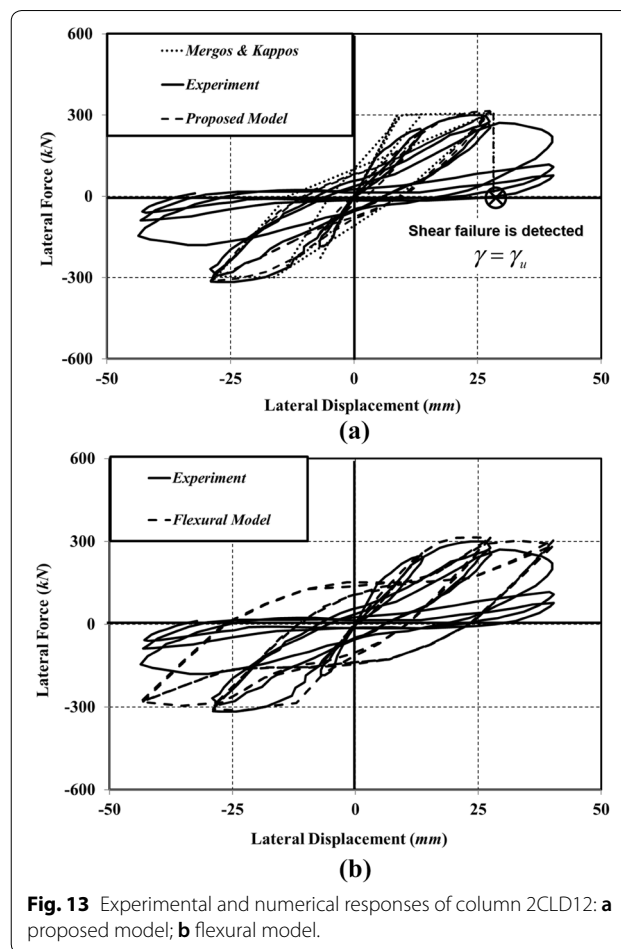
6 Model Validation Against Experimental Evidence

To examine the validity of the proposed RC frame element and to discuss the importance of including shear–flexure interaction effects, three correlation investigations are conducted. The first set considers cyclic tests of two RC columns which eventually failed in shear following flexural yielding and the effects of shear–flexure interaction on both global and local responses are discussed. This type of member is referred to as a “flexure–shear” critical member. The second set studies the cyclic response of an RC column failed in shear before reaching its flexural strength. This type of member is referred to as a “shear” critical member. In all numerical models, 16 proposed elements are used to discretize the column; seven Gauss–Lobatto integration points are used for all elements; and forty fibers (layers) are used to discretize the column cross section. The flexural model proposed by Spacone et al. (1996) is also used to obtain numerical results.

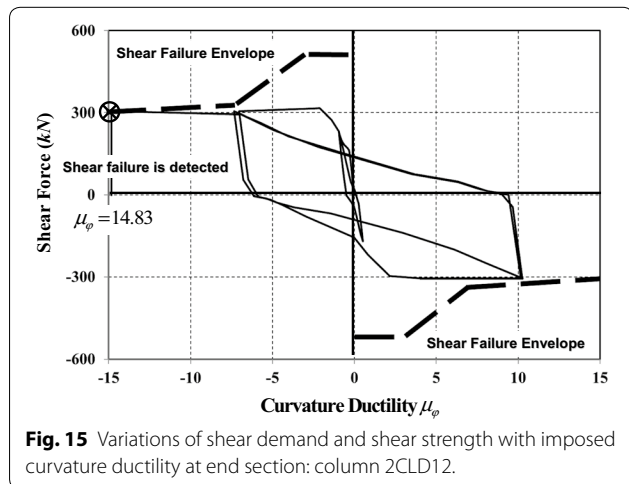
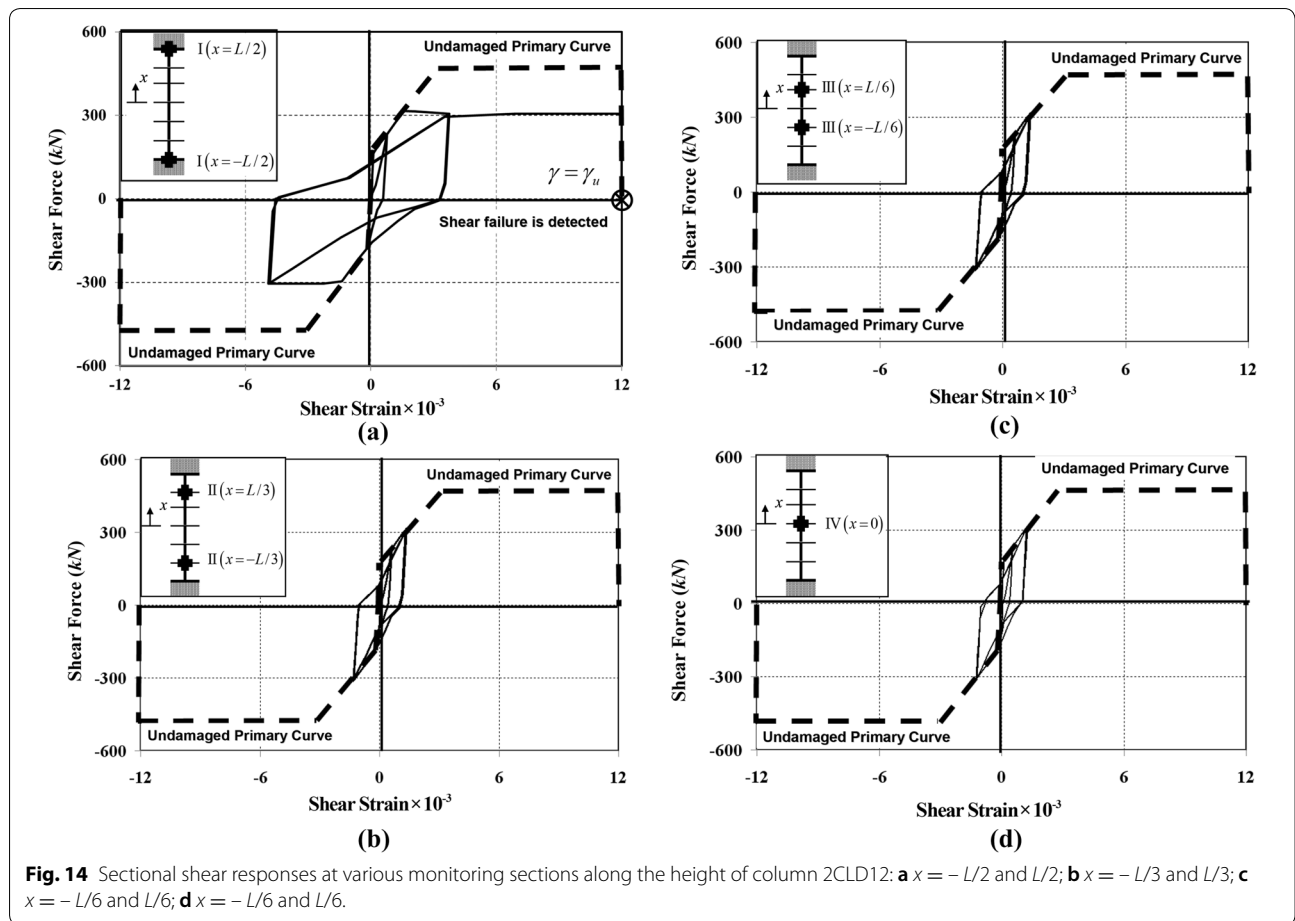
6.1 Flexure–Shear Critical Members

6.1.1 Sezen (2002): Column 2CLD12

Sezen (2002) conducted a series of tests on RC square columns representing older existing columns with sub-standard seismic reinforcement details. One of these columns, labeled column 2CLD12, is modeled by the proposed RC frame element. Mergos and Kappos (2008) used the same column to validate their distributed flexibility frame element with shear–flexure interaction. The geometry, material properties, and reinforcement detail of column 2CLD12 as provided by Sezen (2002) are shown in Fig. 12.



In Fig. 13a the tip load–displacement response from the experimental test is superimposed on the numerical results obtained using both the proposed and the Mergos–Kappos models, while in Fig. 13b the experimental result is compared with the numerical result simulated by the flexural model. Clearly, Fig. 13a shows that the proposed element can represent reasonably well the salient characteristics of the experimental load–displacement behavior. However, the proposed model cannot accurately represent initial stiffness of the experimental load–displacement response since the concrete tensile strength is neglected herein. Compared to the Mergos–Kappos model, the proposed model represents a smoother load–displacement response, thus resulting in a more accurate yielding process in flexure. This benefit is due to the fiber-section model employed to characterize the column section response. It is worth remarking that the Mergos–Kappos model employs the bilinear yield-oriented moment–curvature curve to characterize the column section response, thus failing to capture the smooth yielding process of column cross section in flexure. From the numerical simulation, the proposed model predicts



that the lateral displacement Δ_y and the sectional shear strain γ_y associated with the plastic-hinge formation are approximately 13.80 mm and 1.58×10^{-3} , respectively. Based on the experimental observation (Sezen 2002), the lateral displacement Δ_u at the onset of drastic shear

strength deterioration is 28.0 mm. This value is close to the one given by the numerical model ($\Delta_u = 28.21$ mm). The essence of considering the shear–flexure interaction effect is emphasized in Fig. 13b in which the experimental result is compared with the numerical result simulated by the flexural model. As expected, the flexural model can predict well the column strength. However, shear failure following the plastic-hinge formation cannot be predicted by the flexural model. Thus, the frame element with inclusion of shear–flexure interaction effect is necessary and essential in simulating the response of RC columns prone to flexure–shear failure (ductile shear failure).

Figure 14 shows hysteretic shear responses at various monitoring sections (sections I, II, III, and IV) along the column height. Plastic hinges can merely take place at the column ends (section I) due to restrained conditions at column ends. Thus, the hysteretic shear response at section I located within the plastic-hinge region is different from those at other sections (sections II, III, and IV) located outside the plastic-hinge zone due to the shear–flexure interaction. Figure 14a shows that once the

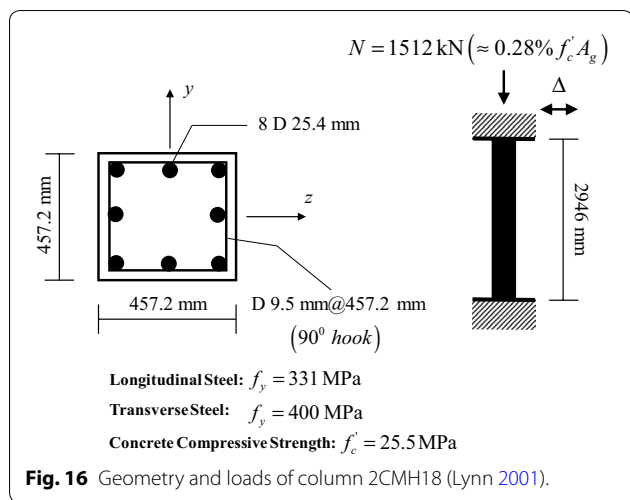


Fig. 16 Geometry and loads of column 2CMH18 (Lynn 2001).

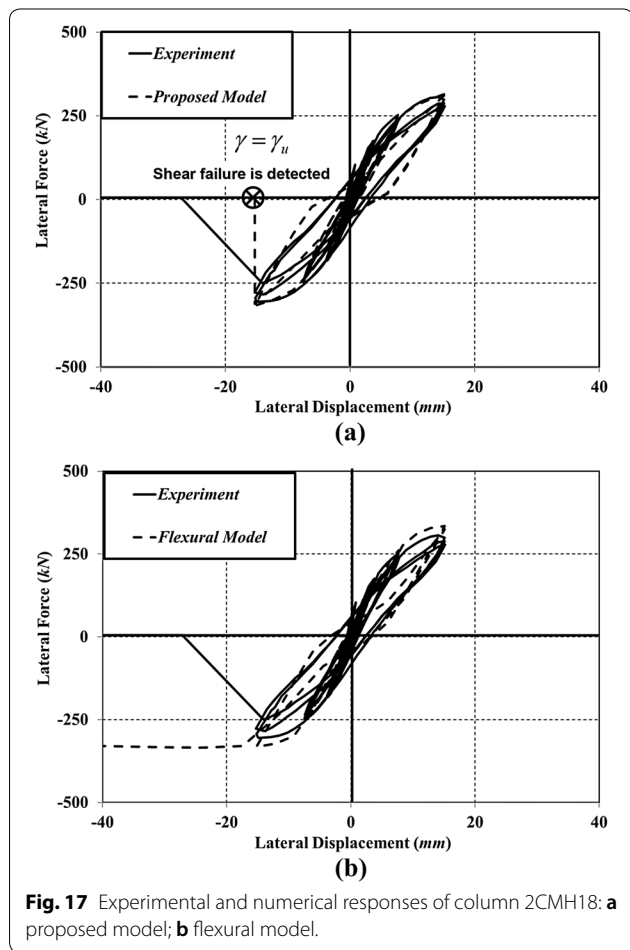


Fig. 17 Experimental and numerical responses of column 2CMH18: **a** proposed model; **b** flexural model.

sectional curvature ductility attains its threshold value of 3, the sectional shear response starts to deviate from the undamaged envelope curve as dictated by the shear–flexure interaction law of the UCSD shear-strength model.

Figure 14b–d show that the hysteretic shear responses at sections II–IV are almost identical. This relies on the fact that the sectional shear–flexure interaction is not activated at sections II, III, and IV since they are located outside the plastic-hinge region. Furthermore, it is observed from Fig. 14 that even though all sections experience the same magnitude of shear force as governed by the equilibrium, the sectional shear strain at section I is much larger than the sectional shear strain at sections II, III, and IV. Eventually, the shear failure is detected at section I when the sectional shear strain attains its ultimate value of $\gamma_u = 12 \times 10^{-3}$. It is worth mentioning that this value is close to the experimental result of 10×10^{-3} as given by Mergos and Kappos (2012).

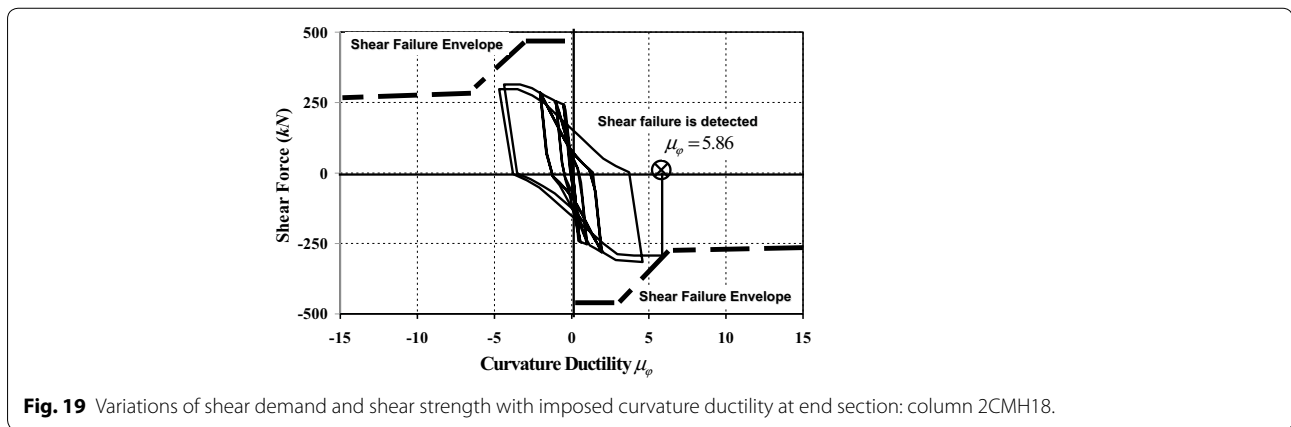
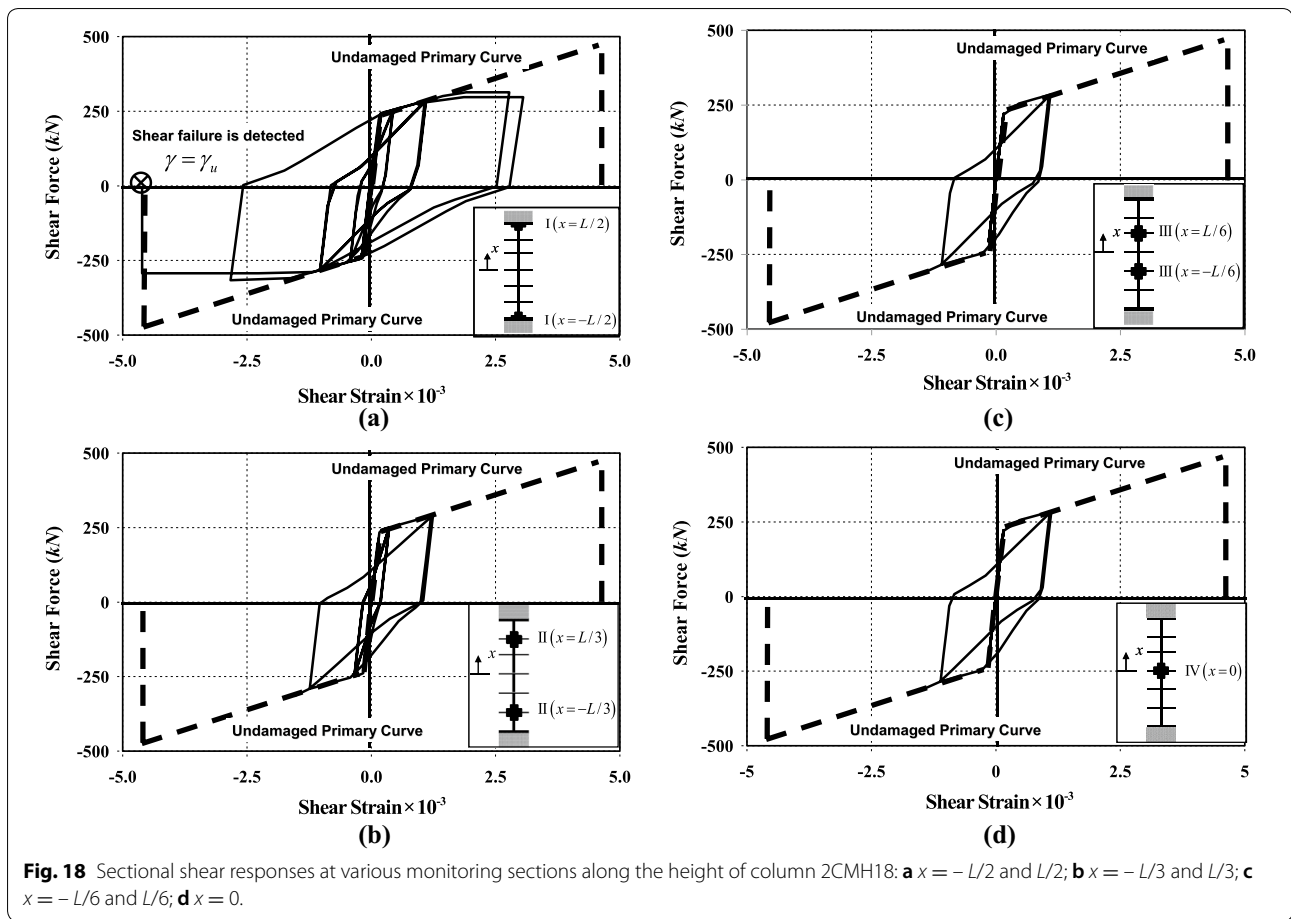
Variations of shear force (demand) and shear strength (capacity) with the curvature ductility at section I are presented in Fig. 15. The shear-strength curve can be considered as the failure envelope and is constructed following the UCSD shear-strength model. The initial shear strength $V_{u0} = 515.6 \text{ kN}$ calculated from Eq. (31) is higher than the peak shear force $V_{\max} = 316.1 \text{ kN}$. If the flexural and shear resisting mechanisms had been independent, column 2CLD12 would not have failed in shear. However, the shear–flexure interaction results in the shear-strength deterioration with increasing curvature ductility ($\mu_\varphi \geq 3$). Column 2CLD12 will eventually fail in shear when the shear demand meets the shear failure envelope with the associated value of the curvature ductility $\mu_\varphi = 14.83$ as shown in Fig. 15.

6.1.2 Lynn (2001): Column 2CMH18

A series of eight RC square columns containing a variety of reinforcement details and subjected to two different levels of axial loading were conducted by Lynn (2001) under cyclic lateral displacements in double bending. These column specimens were constructed to represent existing RC columns built before the 1970s. One of these columns, labeled column 2CMH18, is modeled by the proposed RC frame element.

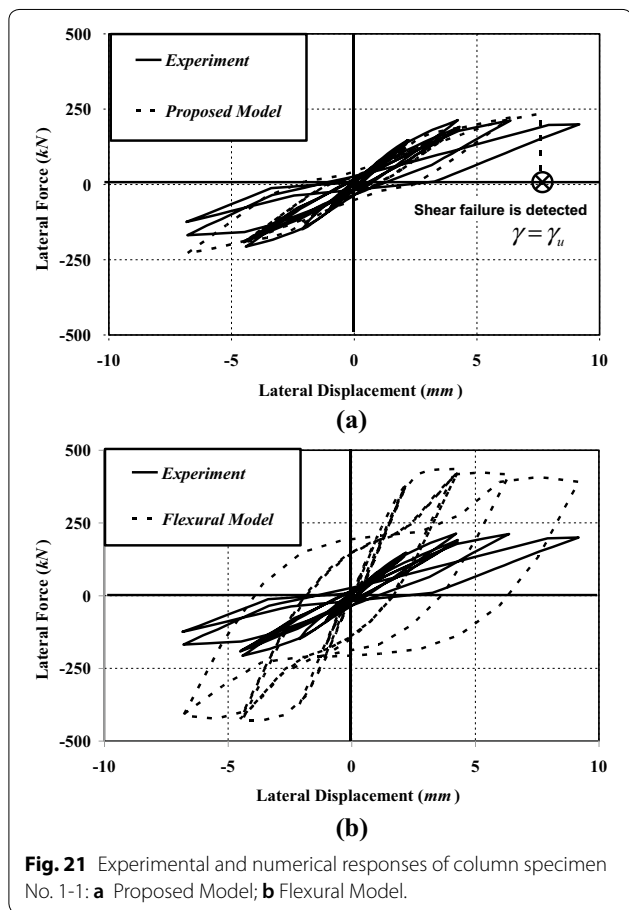
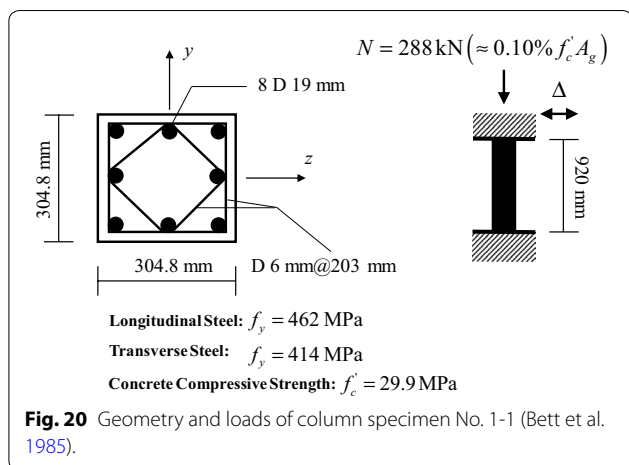
The geometry, material properties and reinforcement detail of column 2CMH18 as provided by Lynn (2001) are shown in Fig. 16. The amount and reinforcing detail of the transverse reinforcement is intended for characterizing the substandard seismic reinforcement details employed before the 1970s.

In Fig. 17a the tip load–displacement response from the experimental test is compared with the numerical result obtained using the proposed model, while in Fig. 17b the experimental result is superimposed on the numerical result obtained using the flexural model. Clearly, both models are capable of characterizing the salient features of the experimental load–displacement response. From Fig. 17a, the proposed model predicts



that the lateral displacement Δ_y and the sectional shear strain γ_y associated with the plastic-hinge formation approximately equal to 8.30 mm and 1.21×10^{-3} , respectively. The lateral displacement Δ_u associated with the ultimate shear strain γ_u is equal to 15.30 mm as obtained by the proposed model. This value of lateral displacement

corresponds well with the experimental observation that the onset of rapid shear strength degradation occurred at lateral displacement of approximately 15.30 mm. Due to the loss of its axial load carrying capacity, the column specimen 2CMH18 eventually collapsed. The importance of including shear–flexure interaction effect



is shown in Fig. 17b in which the experimental result is compared with the numerical result simulated with the flexural model. Although the flexural model can predict reasonably well the general features of the experimental

load–displacement response, shear failure following the plastic-hinge formation cannot be predicted by the flexural model. Consequently, the frame element considering shear–flexure interaction is necessary and essential in the seismic evaluation of RC columns prone to flexure–shear failure (ductile shear failure).

Hysteretic shear responses at various monitoring sections (sections I, II, III, and IV) along the column height are presented in Fig. 18. The hysteretic shear response at section I resting inside the plastic-hinge region is different from those at other sections (sections II, III, and IV) resting outside the plastic-hinge zone due to the shear–flexure interaction. It is worth mentioning that plastic hinges are located only at column ends due to their restrained conditions. Figure 18a indicates that the sectional shear response begins to deviate from the undamaged envelope curve when the sectional curvature ductility reaches its threshold value of 3 as dictated by the shear–flexure interaction law of the UCSD shear-strength model. Figure 18b–d indicate that the hysteretic shear responses at sections II–IV are almost identical. This relies on the fact that the sectional flexure–shear interaction is not activated at sections II, III, and IV since they are located outside the plastic-hinge zone. Comparison between the sectional shear responses in Fig. 18a and Fig. 18b–d indicates that although all sections are subjected to the same magnitude of shear force as governed by the equilibrium, the sectional shear strain at section I is much larger than the sectional shear strains at sections II, III, and IV. Eventually, the shear failure occurs at section I when the sectional shear strain reaches its ultimate value of $\gamma_u = 4.6 \times 10^{-3}$. It is worth remarking that for the transverse reinforcement detail of the column specimen 2CMH18, the shear strain γ_{st} corresponding to the verge of transverse reinforcement yielding and the shear strain γ_u corresponding to the onset of shear failure (significant strength deterioration) are equal based on the undamaged primary curve proposed by Mergos and Kappos (2012).

Figure 19 shows the variations of shear force (demand) and shear strength (capacity) with the curvature ductility at section I. The shear-strength curve based on the UCSD shear-strength model can be regarded as the failure envelope. The initial shear strength $V_{u0} = 477.2 \text{ kN}$ calculated from Eq. (31) is higher than the peak shear force $V_{max} = 316.0 \text{ kN}$. If the shear–flexure interaction had not been considered, the column 2CMH18 would not have failed in shear. However, the shear–flexure interaction results in the shear-strength deterioration with increasing curvature ductility ($\mu_\phi \geq 3$). Figure 19 shows that column 2CMH18 will eventually fail in shear when the shear demand meets the shear failure envelope with

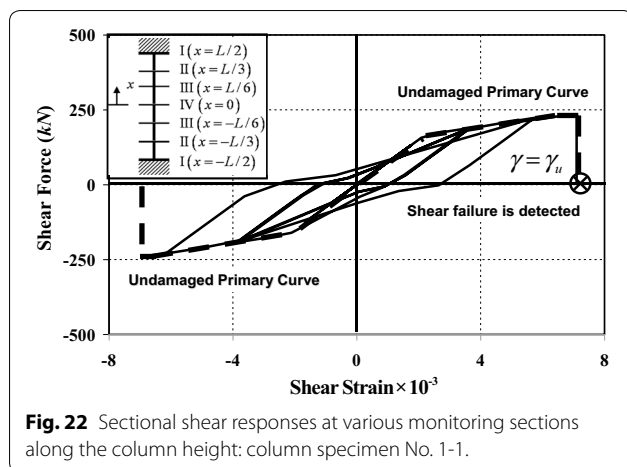


Fig. 22 Sectional shear responses at various monitoring sections along the column height: column specimen No. 1-1.

the associated value of the curvature ductility $\mu_\phi = 5.86$. When compared to column 2CMH18 (Lynn 2001) presently studied, column 2CLD12 (Sezen 2002) discussed previously experiences shear failure at a much larger value of curvature ductility ($\mu_\phi = 14.83$). This observation relies on the fact that column 2CMH18 was subjected to a higher axial loading and was on a more ductile sectional shear envelope of the column 2CLD12.

6.2 Shear Critical Member

6.2.1 Bett et al. (1985): Column Specimen No. 1-1

A series of two-thirds scale RC columns with square cross section was tested by Bett et al. (1985) to assess the efficiency of strengthening and repairing techniques for short columns designed in seismic regions of the US in the 1950s and 1960s. One of these columns, labeled Specimen No. 1-1, is used herein to examine the validity of the proposed RC frame element in modeling a shear-dominated (shear critical) column. Figure 20 shows the geometry, material properties, and reinforcement detail of column specimen No. 1-1 as provided by Bett et al. (1985).

In Fig. 21a the tip load–displacement response from the experimental test is superimposed on the numerical result obtained using the proposed model, while in Fig. 21b the experimental result is compared with the numerical result simulated by the flexural model. Figure 21a shows that the proposed element can predict well the salient characteristics of the experimental load–displacement response. Unlike the load–displacement responses of flexural–shear critical members (column 2CLD12 and column 2CMH18) previously investigated, pinching of the hysteretic loops can be clearly noticed in the load–displacement response of column No. 1-1. This is expected since column No. 1-1 is considered a shear-dominated member. From

Fig. 21a, the proposed model predicts that lateral displacement Δ_u and sectional shear strain γ_u corresponding to the onset of drastic shear strength deterioration equal to 7.6 mm and 7.10×10^{-3} , respectively, and there is no plastic-hinge formation in column No. 1-1. This prediction corresponds well with the experimental observation. Figure 21b shows the adverse consequence of considering only flexural response in the numerical simulation. Clearly, the flexural model fails to simulate the load–displacement response of column No. 1-1. With the flexural model, both the member strength and the amount of dissipated hysteretic energy are drastically overestimated. Consequently, frame element with inclusion of sectional shear response is necessary and essential in assessing seismic performance of the shear-dominated RC columns.

Hysteretic shear responses at various monitoring sections (sections I, II, III, and IV) along the column length are presented in Fig. 22. Unlike the sectional shear responses of column 2CLD12 and column 2CMH18, the hysteretic shear responses at all monitoring sections of column No. 1-1 are identical. This relies on the fact that all column sections have not experienced yielding in flexure. Consequently, sectional shear–flexure interaction is not triggered in column No. 1-1 and the hysteretic shear responses follow the undamaged primary curve. The pinching characteristic is noticeable in the sectional shear response. Eventually, shear failure takes place once the sectional shear strain attains its ultimate value of $\gamma_u = 7.10 \times 10^{-3}$.

7 Summary and Conclusions

The present work proposes a fiber frame element for an inelastic analysis of reinforced concrete (RC) members prone to flexure–shear failure as well as shear failure. The proposed frame element is constructed within the framework of stiffness-based model and relies on the Timoshenko beam kinematics assumption, thus leading to comparatively simple and readily implemented equations. The choice of displacement interpolation functions is selected with care to obtain the locking-free Timoshenko frame element. Material nonlinearities are considered in the uniaxial hysteretic laws for concrete, steel, and sectional shear. Adverse influences of inelastic flexural deformation (plastic-hinge formation) on shear capacity are accounted for within the framework of the UCSD shear-strength model. The numerical procedure for shear–flexure interaction is modified following the Mergos–Kappos procedure. The model inputs are based on general engineering properties of RC members. The proposed element is simple, computationally efficient and able to describe several distinct characteristics of

non-ductile RC column responses. Accuracy of the proposed model is validated through correlation studies on non-ductile RC columns under cyclic loadings.

For flexure–shear critical columns, the proposed model can predict reasonably well the member strength, stiffness deterioration with larger displacement magnitude, the amount of dissipated hysteretic energy, the general shape of hysteretic response, and the failure mode. The proposed model can represent well the shear-strength deterioration and the drastic increase of shear deformations after plastic-hinge formation. The essence of including the shear–flexure interaction is further emphasized when the flexural model is used to simulate the experimental response.

For the shear critical column, the proposed model can represent reasonably well the member strength, stiffness deterioration with larger displacement magnitude, the amount of dissipated hysteretic energy, the general pinched shape of the hysteretic response, and the failure mode. The essence of including shear response is confirmed when the flexural model is replaced by the proposed model.

Authors' contributions

WS plays a role in implementing the numerical model, collecting the experimental data, interpreting the numerical results, and partially writing the manuscript; SL plays a role in formulating the numerical model, collecting the experimental data, interpreting the numerical results and partially writing the manuscript; WP plays a role in interpreting the numerical results and partially writing the manuscript; SH plays a role in interpreting the numerical results and revising the manuscript; and PP plays a role in interpreting the numerical results. All authors read and approved the final manuscript.

Author details

¹ Department of Civil Engineering, Faculty of Engineering, Prince of Songkla University, Songkhla 90112, Thailand. ² School of Civil Engineering and Center of Excellence in Innovation for Sustainable Infrastructure Development, Suranaree University of Technology, Nakhon Ratchasima, Thailand.

Acknowledgements

This study was partially supported by the Thailand Research Fund (TRF) under Grant RTA5980005, by the STREAM Research Group under Grant ENG-51-2-7-11-022-S, Faculty of Engineering, Prince of Songkla University, and by Scholarship Awards for Thai Ph.D. Students under Thailand's Education Hub for Southern Region of ASEAN Countries and Scholarship from Faculty of Engineering, Prince of Songkla University. Opinions expressed in this paper are those of the authors and do not reflect the views of the sponsoring agencies. Special thanks go to a senior lecturer Mr. Wiwat Sutiwipakorn for reviewing and correcting the English of this paper. Additionally, the authors would also like to thank anonymous reviewers for their valuable and constructive comments.

Competing interests

The authors declare that they have no competing interests.

Availability of data and materials

All experimental data employed in this work can be found in the following references: Bett et al. (1985); Lynn (2001); and Sezen (2002).

Funding

Thailand Research Fund (TRF) under Grant RTA5980005. STREAM Research Group under Grant ENG-51-2-7-11-022-S, Faculty of Engineering, Prince of Songkla University. Scholarship Awards for Thai Ph.D. Students under

Thailand's Education Hub for Southern Region of ASEAN Countries and Scholarship from Faculty of Engineering, Prince of Songkla University.

Publisher's Note

Springer Nature remains neutral with regard to jurisdictional claims in published maps and institutional affiliations.

Received: 13 June 2018 Accepted: 2 April 2019

Published online: 03 June 2019

References

- Aboutaha, R. S., Engelhardt, M. D., Jirsa, J. O., & Kreger, M. E. (1999). Rehabilitation of shear critical concrete columns by use of rectangular steel jackets. *ACI Structural Journal*, *96*(1), 68–78.
- Bett, B., Klinger, R., & Jirsa, J. O. (1985). Behavior of strengthened and repaired R/C columns under cyclic deformations. PMFSEL report no 85-3, University of Texas, Austin, USA.
- Ceresa, P., Petrini, L., & Pinho, R. (2007). Flexure–shear fiber beam–column elements for modeling frame structures under seismic loading: State of the art. *Journal of Earthquake Engineering*, *11*(supplement 1), 46–88.
- Ceresa, P., Petrini, L., Pinho, R., & Sousa, R. (2009). A fibre flexure–shear model for seismic analysis of RC-framed structures. *Earthquake Engineering and Structural Dynamics*, *38*(5), 565–586.
- Filippou, F. C., D'Ambrisi, A., & Issa, A. (1992). Nonlinear static and dynamic analysis of reinforced concrete subassemblages. Earthquake Engineering Research Center Report No. UCB/EERC-92/08, University of California, Berkeley, USA.
- Fraeijns de Veubeke, B. M. (1965). Displacement and equilibrium models. Chapter 9 in *Stress Analysis* (pp. 145–197), Wiley, London.
- Gerin, M., & Adebar, P. (2004). Accounting for shear in seismic analysis of concrete structures. In *Proceeding of 13th World Conference on Earthquake Engineering*, Vancouver, paper no. 1747.
- Ghee, A., Priestley, M. J. N., & Paulay, T. (1989). Seismic shear strength of circular reinforced concrete columns. *ACI Structural Journal*, *86*(1), 45–59.
- Giberson, M. F. (1967). *The response of nonlinear multi-story structures subjected to earthquake excitation*. Pasadena: Earthquake Engineering Research Laboratory, California Institute of Technology.
- Kagermanov, A., & Ceresa, P. (2016). Physically based cyclic tensile model for RC membrane elements. *Journal of Structural Engineering*, *142*(12), 04016118.
- Kagermanov, A., & Ceresa, P. (2017). Fiber-section model with an exact shear strain profile for two-dimensional RC frame structures. *Journal of Structural Engineering*, *143*(10), 04017132.
- Kent, D. C., & Park, R. (1971). Flexural members with confined concrete. *ASCE Journal of Structural Division*, *97*(7), 1964–1990.
- Kim, J., Kwon, M., Jung, W., & Limkatanyu, S. (2013). Seismic performance evaluation of RC columns reinforced by GFRP composite sheets with clip connectors. *Construction and Building Materials*, *43*, 563–574.
- Li, X., Park, R., & Tanaka, H. (1995). Reinforced concrete columns under seismic lateral force and varying axial load. Research Report 95-5, Department of Civil Engineering, University of Canterbury, Christchurch, New Zealand.
- Limkatanyu, S., & Spacone, E. (2002). Reinforced concrete frame element with bond interfaces. I: Displacement-based, force-based, and mixed formulations. *Journal of Structural Engineering*, *128*(3), 346–355.
- Lynn, A. C. (2001). Seismic evaluation of existing reinforced concrete building columns. Ph.D. thesis, Department of Civil and Environmental Engineering, University of California, Berkeley, USA.
- Lynn, A. C., Moehle, J. P., Mahin, S. A., & Holmes, W. T. (1996). Seismic evaluation of existing reinforced concrete building columns. *Earthquake Spectra*, *12*(4), 715–739.
- Ma, S. M., Bertero, V. V., & Popov, E. P. (1976). Experimental and analytical studies on hysteretic behavior of RC rectangular and T-beam. Earthquake Engineering Research Center Report No. UCB/EERC-76/02, University of California, Berkeley, USA.
- Marini, A., & Spacone, E. (2006). Analysis of reinforced concrete elements including shear effects. *ACI Structural Journal*, *103*(5), 645–655.
- Martino, R. (1999). Nonlinear Pushover Analysis of Reinforced Concrete Structures. Mater thesis, Department of Civil, Environmental, Architectural Engineering, University of Colorado, Boulder, USA.

- Menegotto, M., & Pinto, P. E. (1973). Method of analysis for cyclically loaded reinforced concrete plane frames including changes in geometry and inelastic behavior of elements under combined normal force and bending. In *Proceeding of IABSE Symposium on Resistance and Ultimate Deformability of Structures Acted on by Well-Defined Repeated Loads*, Lisbon (pp. 17–22).
- Mergos, P. E., & Kappos, A. J. (2008). A distributed shear and flexural flexibility model with shear–flexure interaction for R/C members subjected to seismic loading. *Earthquake Engineering and Structural Dynamics*, 37(12), 1349–1370.
- Mergos, P. E., & Kappos, A. J. (2012). A gradual spread inelasticity model for R/C beam–columns, accounting for flexure, shear and anchorage slip. *Engineering Structures*, 44, 94–106.
- Moehle, J. P., & Mahin, S. A. (1991). Observations on the behavior of reinforced concrete buildings during earthquakes. ACI SP-127: Earthquake-Resistant Concrete Structures Inelastic Response and Design, American Concrete Institute, Detroit.
- Moehle, J. P., Sezen, H., & Elwood, K. J. (2001). Response of reinforced concrete buildings lacking details for ductile response. In *Proceeding of 4th International Symposium on Earthquake Engineering for the Moderate Seismicity Regions* (pp. 117–131).
- Onate, E. (2013). *Structural analysis with the finite element method volume 2: beams, plates and shells*. Netherlands: Springer.
- Ozbolt, J., & Bazant, Z. P. (1992). Microplane model for cyclic triaxial behavior of concrete. *Journal of Engineering Mechanics*, 118(7), 1365–1386.
- Palermo, D., & Vecchio, F. J. (2003). Compression field modeling of reinforced concrete subjected to reversed loading: Formulation. *ACI Structural Journal*, 100(5), 616–625.
- Panto, B., Rapicavoli, D., Caddemi, S., & Calio, I. (2017). A smart displacement based (SDB) beam element with distributed plasticity. *Applied Mathematical Modeling*, 44, 1339–1351.
- Park, R., & Paulay, T. (1975). *Reinforced concrete structures*. New York: Wiley.
- Petrangeli, M., Pinto, P. E., & Ciampi, V. (1999). Fiber element for cyclic bending and shear of RC structures. I: Theory. *Journal of Engineering Mechanics*, 125(9), 994–1001.
- Pincheira, J. A., Dotiwala, F. S., & D'Souza, J. T. (1999). Seismic analysis of older reinforced concrete columns. *Earthquake Spectra*, 15(2), 245–272.
- Priestley, M. J. N., Seible, F., Verma, R., & Xiao, Y. (1993). Seismic shear strength of reinforced concrete columns. Structural Systems Research Project Report No. SSRP 93/06, University of California, San Diego, USA.
- Ranzo, G., & Petrangeli, M. (1998). A fibre finite beam element with section shear modelling for seismic analysis of RC structures. *Journal of Earthquake Engineering*, 2(3), 443–473.
- Ricles, J. M., Yang, Y. S., & Priestley, M. J. N. (1998). Modeling nonductile R/C columns for seismic analysis of bridges. *Journal of Structural Engineering*, 124(4), 415–425.
- Sezen, H. (2002). Seismic behavior and modeling of reinforced concrete building columns. Ph.D. thesis, Department of Civil and Environmental Engineering, University of California, Berkeley, USA.
- Sezen, H. (2008). Shear deformation model for reinforced concrete columns. *Structural Engineering and Mechanics*, 28(1), 39–52.
- Sezen, H., & Moehle, J. P. (2004). Shear strength model for lightly reinforced concrete columns. *Journal of Structural Engineering*, 130(11), 1692–1703.
- Sezen, H., Whittaker, A. S., Elwood, K. J., & Mosalam, K. M. (2003). Performance of reinforced concrete buildings during the August 17, 1999 Kocaeli, Turkey earthquake, and seismic design and construction practise in Turkey. *Engineering Structures*, 25(1), 103–114.
- Soleimani, D. (1978). Reinforced concrete ductile frames under earthquake loadings with stiffness degradation, Ph.D. thesis, University of California, Berkeley, USA.
- Spacone, E., Filippou, F. C., & Taucer, F. F. (1996). Fiber beam–column model for nonlinear analysis of R/C frames. Part I: Formulation. *Earthquake Engineering and Structural Dynamics*, 25(7), 711–725.
- Spacone, E., & Limkatanyu, S. (2000). Responses of reinforced concrete members including bond-slip effects. *ACI Structural Journal*, 97(6), 831–839.
- Taylor, R. L. (2000). FEAP: A finite element analysis program, User manual: version 7.3. Department of Civil and Environmental Engineering, University of California, Berkeley, USA.

Submit your manuscript to a SpringerOpen® journal and benefit from:

- Convenient online submission
- Rigorous peer review
- Open access: articles freely available online
- High visibility within the field
- Retaining the copyright to your article

Submit your next manuscript at ► [springeropen.com](https://www.springeropen.com)
